JGR Space Physics

RESEARCH ARTICLE
10.1029/2022JA030870

**Key Points:**

- The dependencies of global positioning system scintillation indices on plasma flow and total electron content (TEC) variation were evaluated around the dawn sector of polar ionosphere
- The phase scintillation index depends linearly only on the plasma flow speed and the rate of change of TEC
- However, the amplitude scintillation index does not rely on the plasma flow and also the rate of change of TEC

**Correspondence to:**
Q.-H. Zhang,
zhangqinghe@sdu.edu.cn

**Citation:**
Wang, Y., Jayachandran, P. T., Ma, Y.-Z., Zhang, Q.-H., Xing, Z.-Y., Ruohoniemi, J. M., et al. (2022). Dependencies of GPS scintillation indices on the ionospheric plasma drift and rate of change of TEC around the dawn sector of the polar ionosphere. *Journal of Geophysical Research: Space Physics*, *127*, e2022JA030870. https://doi.org/10.1029/2022JA030870

Received 23 JUL 2022
Accepted 17 OCT 2022



# Dependencies of GPS Scintillation Indices on the Ionospheric Plasma Drift and Rate of Change of TEC Around the Dawn Sector of the Polar Ionosphere

**Y. Wang[1], P. T. Jayachandran[2], Y.-Z. Ma[1], Q.-H. Zhang[1], Z.-Y. Xing[1], J. M. Ruohoniemi[3], S. G. Shepherd[4], and M. Lester[5]**

[1]Shandong Provincial Key Laboratory of Optical Astronomy and Solar-Terrestrial Environment, Institute of Space Sciences, Shandong University, Weihai, China, [2]Physics Department, University of New Brunswick, Fredericton, NB, Canada, [3]Bradley Department of Electrical and Computer Engineering, Virginia Tech, Blacksburg, VA, USA, [4]Thayer School of Engineering, Dartmouth College, Hanover, NH, USA, [5]Department of Physics and Astronomy, University of Leicester, Leicester, UK

**Abstract** The dependencies of global positioning system (GPS) scintillation indices on ionospheric plasma flow and the rate of change of total electron content (TEC) around the dawn sector for the first time of the polar ionosphere are investigated. The phase scintillation index ($\sigma_\varphi$) derived from GPS measurements of the Canadian High Arctic Ionospheric Network (CHAIN) shows linear dependencies on both the plasma drift speed measured by the SuperDARN radar and on the rate of change of TEC estimated from the GPS receivers of CHAIN. However, the amplitude scintillation index ($S_4$) does not show any dependence on the plasma flow or the rate of change of TEC. These results further support Wang et al. (2018), https://doi.org/10.1002/2017JA024805 at the noon sector. The dependence of the phase scintillation index on the plasma flow further evidences that the standard phase scintillation index is dominated by refractive variations due to the use of a fixed cut-off frequency of 0.1 Hz while detrending the phase observable. The dependence of the phase scintillation index on the rate of change of TEC consolidates the dominance of refractive variations inside.

**Plain Language Summary** In decades, the standard scintillation indices are widely used to represent the strength of scintillations in the ionosphere, which were usually calculated from the sixth order Butterworth filter with a fixed cut-off frequency of 0.1 Hz by the ground-based Global Navigation Satellite System (GNSS) receiver automatically. At middle-to-low latitudes, the applications of these indices are working very well. However, over the polar ionosphere, the completely different scintillation phenomenon "Phase without Amplitude" occurred when confronting the hazard conditions. Then, in order to explaining this weird, many researchers have carried out a lot of valuable approaches, fundamentally challenging the direct adopt of standard phase scintillation index. Here, for the first time, we present an experimental evidence on the dawn sector to prove the clear positive dependence of phase scintillation index on the convection flow speed and also the TEC variations. It reminds us to be careful when using the standard phase scintillation index over the polar region, in particular with high-speed flows.

## 1. Introduction

When a radio wave propagates through the ionosphere, the incident signal is affected by the presence of plasma irregularities with various temporal and spatial scales, giving rise to the scintillations (e.g., Hey et al., 1946; Mitchell et al., 2005; Moen et al., 2013; Wang et al., 2021, 2016; Weber et al., 1986). The scintillation is generally quantified using two types of indices: the phase scintillation index ($\sigma_\varphi$, standard deviation of the phase calculated in a specific time interval) and the amplitude scintillation index ($S_4$, normalized standard deviation of the amplitude in a given interval).

In order to obtain these scintillation indices from Global Navigation Satellite System (GNSS), such as global positioning system (GPS)/BeiDou observables, the long-term trends in the signal should be removed, which are the variations with frequencies slower than 0.1 Hz in the context. These long-term trends include variations in the background of ionosphere, the Doppler shift due to the satellite-receiver relative motion, and some hardware deviations (such as the clock drift). Usually, the receivers perform an automated process to apply a sixth order Butterworth filter with a fixed cut-off frequency of 0.1 Hz (e.g., Materassi et al., 2009; van der Meeren et al., 2014). The standard cut-off frequency of 0.1 Hz was statistically derived from wideband satellite

measurements at low latitudes (Fremouw et al., 1978), which is closely to be the Fresnel frequency (e.g., Van Dierendonck et al., 1993). However, the use of this fixed cut-off frequency for the high latitude region leads to the inclusion of phase variations that are not associated with the scintillation phenomena in the calculation of the phase scintillation index (e.g., Beach, 2006; Forte, 2005; Forte & Radicella, 2002; van der Meeren et al., 2014; Wang et al., 2018). Moreover, McCaffrey and Jayachandran (2019) have shown that these variations are refractive in nature.

In decades, a significant number of researchers have focused on the generations and dynamics of scintillation phenomena, continually refreshing our general understanding of the physics of scintillation. As far as we know, the classic phase scintillation index ($\sigma_\varphi$) includes two fundamental different variations: (a) diffractive variations, which are stochastic in nature and therefore cannot be mitigated easily; (b) refractive variations, which are deterministic in nature and can be corrected by using multi-frequency measurements. On the contrary, the standard amplitude scintillation index ($S_4$) almost stems from diffractive variations. This viewpoint has been comprehensively studied not only in theory but also by experiments especially over the polar region (e.g., Beach, 2006; Carrano et al., 2016; Forte, 2005; Forte & Radicella, 2002; Jayachandran et al., 2017; McCaffrey & Jayachandran, 2019; Mushini et al., 2012; Wang et al., 2018), which explained the non-physical phenomenon of "Phase without Amplitude" scintillations at high latitudes (e.g., Doherty et al., 2003; Li et al., 2010; Pi et al., 2001).

In theory, Forte and Radicella (2002) and Beach (2006) challenged the presumed applicability of the fixed cut-off frequency (0.1 Hz) at high latitudes, which is always thought of as the Fresnel frequency. Wang et al. (2018) reported the first evidence to prove the strong linear dependence of $\sigma_\varphi$ on the ionospheric plasma drift rather than $S_4$ around the noon sector. Moreover, to distinguish the rapid refractive variations from the diffractive effects, usually both making up the phase scintillation represented by the standard $\sigma_\varphi$, McCaffrey and Jayachandran (2019) developed a new tool to determine the Fresnel frequency roughly by using high-rate carrier phase observations on both the L1 and L2 carriers independently. For further understanding, it is worth extensively studying the polar region to discover the potential relations of these standard phase and amplitude scintillation indices on ionospheric parameters, such as the ionospheric plasma flow and the rate of change of total electron content (TEC).

In this article, we present further observational evidence to demonstrate the relationships of the scintillation indices on the plasma flow velocity and the rate of change of TEC around the dawn sector of high latitudes, by using measurements from the GPS receivers of the Canadian High Arctic Ionospheric Network (CHAIN) (Jayachandran et al., 2009), and the SuperDARN radars of Blackstone (BKS), Fort Hays West (FHW), and Christmas Valley East (CVE) (Chisham et al., 2007; Greenwald et al., 1995).

## 2. Instruments and Measurements

In this study, the scintillation data is obtained from the ground-based GPS receivers of the CHAIN over the Canadian Arctic, which currently consists of 29 GPS receivers, with a sampling rate of 50 Hz or 100 Hz. Here, we used the data from Novatel GSV4004B receivers with a sampling rate of 50 Hz, covering a very large area in the polar region. To represent amplitude and phase scintillations, the standard phase scintillation index ($\sigma_\varphi$) and amplitude scintillation index ($S_4$) were used in a cadence of 1 min, which had been automatically processed by using a sixth order Butterworth filter with a fixed cut-off frequency of 0.1 Hz in order to remove the long-period trends as mentioned in Section 1. In this article, the standard processing progress is employed to review the dependencies of phase scintillation index on various parameters (e.g., the plasma flow, and the rate of change of TEC). The same methodology is applied to the amplitude scintillations as well to delineate the diffractive and refractive effects. In order to avoid most of the multi-path effects, GPS measurements whose elevation angles lower than 20° are masked.

The measurements of ionospheric plasma flow are provided by SuperDARN radars, which currently consist of more than 30 high-frequency (HF) radars extending over a vast area from mid-latitudes to high-latitudes in both hemispheres (Chisham et al., 2007). Through Doppler shifts in the backscattered signal, SuperDARN radar detects the movement of ionospheric irregularities with decameter scales along line-of-sight (LOS) directions of the corresponding radar beams. By combining Doppler measurements along LOS directions from more than two SuperDARN radars, the vector of plasma velocity can be well estimated using the global fitting technique referred to as the map potential (Ruohoniemi & Baker, 1998; Shepherd & Ruohoniemi, 2000). The velocity data

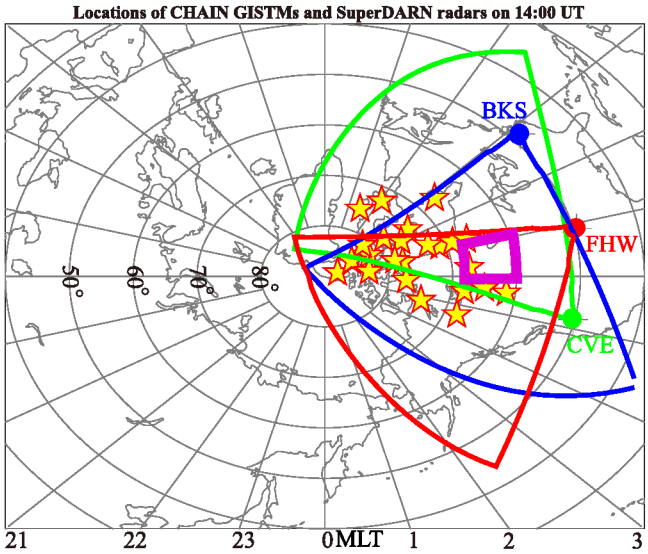


**Figure 1.** The distribution of Canadian High Arctic Ionospheric Network (CHAIN) global positioning system (GPS) receivers (marked by yellow stars with red edge) and the field-of-view (FOV) of SuperDARN radars of Blackstone (BKS, solid blue), Fort Hays West (FHW, solid red), and Christmas Valley East (CVE, solid green) under magnetic latitude (MLat)/magnetic local time (MLT) coordinate system with noon on the top and dawn on the right at 14:00 UT. In this study, the selected region is highlighted by the bold solid magenta frame at the dawn sector of Canadian arctic, covering a range of 60°–68° MLat and 06:00–07:00 MLT during a time period of 13:00–15:00 UT.

from SuperDARN radars are provided at a cadence of 2 min and a spatial scale of 1° magnetic latitude (MLat) × 2° magnetic longitude (MLon) under Altitude-Adjusted Corrected Geomagnetic Coordinates (AACGM).

To focus on the dawn sector of high latitudes, a particular region is picked out deliberately, which ranges between 60° and 68° MLat and 06:00–07:00 magnetic local time (MLT) using AACGM. We have focused on the Canadian sector at where the CHAIN is located by selecting the time interval between 13:00 UT and 15:00 UT. Around this region, the plasma drift is probably the regular sunward return flow and/or the dawnside auroral polarization streams (DAPS) with high speeds (e.g., Liu et al., 2020; Wang et al., 2020; Zhang et al., 2013). The selected region is defined by the following criterions: (a) a number of GPS receivers around the selected region to provide plentiful ray paths; (b) high occurrence rate of high-speed plasma flow in the selected region; (c) significant amount of back scatters from several SuperDARN radars to merge flow vectors in the selected region. For this study, the selected region is well overlapped simultaneously by GPS receivers of CHAIN and SuperDARN radars located at Blackstone, VA (BKS), Fort Hays, KS (FHW), and Christmas Valley, Oregon (CVE), respectively.

Figure 1 provides an overview of the distribution of GPS receivers of CHAIN (yellow stars with red margins) and the field-of-views (FOVs) of the BKS (solid line in green), FHW (solid line in red), and CVE (solid line in blue) SuperDARN radars in the MLat/MLT grids under AACGM at 14:00 UT. Noon MLT is on top with dawn to the right. The magenta frame (bold solid line) highlights the region of 60°–68° MLat and 06:00–07:00 MLT, referred to as "the selected region" herein.

## 3. Results

### 3.1. The Dependence of Phase Scintillation Index on Plasma Drift Speed

In order to investigate the dependence of scintillation indices on plasma flow at the dawn sector over the polar ionosphere, a statistical study was carried out over a period of 3 years from 2013 to 2015 by using the available data from the selected region (60°–68° MLat and 06:00–07:00 MLT). For comparing the data of CHAIN GPS receiver (e.g., scintillation indices, TEC variations) with the SuperDARN velocity, the receiver measurements were projected into uniform grids (1° MLat × 8 min MLT) on Ionospheric Pierce Point at an assumed altitude of 350 km (approximately the peak height of F2 layer of the ionosphere). After that, the corresponding data triads have been constructed, each consisting of the specific scintillation index and velocity and rate of change of TEC. Note that the data contained by each data triad approximately overlap one point within the selected region. Please refer to Wang et al. (2016, 2018) for a detailed description of the data processing. The data triads whose scintillation indices below 0.05 have been discarded due to the noise level definition of the receiver. In order to process a considerable amount of extracted data triads within the two datasets (both comprising of ~65,000 data triads), the two datasets have been grouped into velocity bins of 5 m/s and then averaged the contained parameters of $\sigma_\varphi$ and $S_4$ in each velocity bin. The number threshold of data triads in each speed container is set as 25 arbitrarily. Figure 2 presents the relations between scintillation indices ($y$-axis) and the velocity speed of plasma flow ($x$-axis); Figure 2a is for $\sigma_\varphi$, and Figure 2b is for $S_4$. In Figure 2, the red squares show the averaged scintillation indices within the corresponding velocity bins and their standard errors in each bin noted by blue vertical lines. The solid black lines in Figures 2a and 2b represent the linear least-square fitting lines based on the average values in each bin, with the equation for the best fit and the correlation coefficient.

From Figure 2a, the averaged $\sigma_\varphi$ is linearly increasing with the growing velocity speed (the best-fit slope is 0.11), accompanied by a high degree of correlation coefficient of 0.87. However, in Figure 2b, the mean values of $S_4$ are always around 0.08 (the best-fit slope is around 0), disregarding the plasma speed of 0.1 km/s or 0.6 km/s.

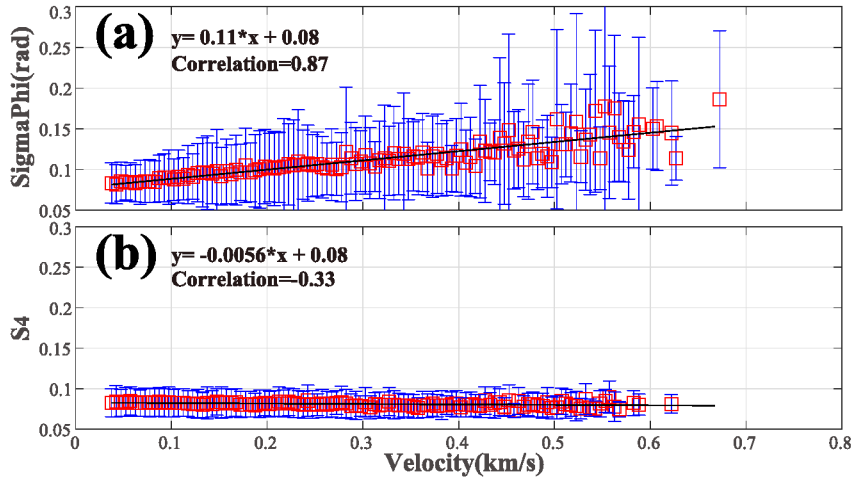


**Figure 2.** The statistical relationships of the phase and amplitude scintillation indices along with the flow velocity speed during a period of 3 years from 2013 to 2015. The velocity speed is binned into 5 m/s bins with a number threshold of 25. The red symbols of boxes are averaged scintillation indices in each bin and blue error bars are standard deviations. The line of best fit to the averages are shown, as well as their equations and correlation coefficients.

As measured by the slopes of the best fits, it is evident that the strength of dependence on plasma drift speed for $\sigma_\varphi$ (0.11) is entirely different from that with $S_4$ (~0). It is a strong experimental evidence, for the first time in the dawn sector, to the clear dependence of phase scintillation index on the relative flow speed and the propagation geometry, which was forecasted by Rino (1979) and was then qualified by Forte and Radicella (2002). Meanwhile, the result is consistent with the dependence investigations around the noon sector (Wang et al., 2018). Moreover, these peculiar characteristics of $\sigma_\varphi$ and $S_4$ from GPS measurements have been employed to predict zonal irregularity drift through the scintillation theory of weak scatter (Carrano et al., 2016). Notably, the no dependence of $S_4$ on the drift speed is highlighted. Note that in this study, only the strength of the plasma drift velocity is used. As mentioned by previous studies (e.g., Forte, 2005; Forte & Radicella, 2002; McCaffrey & Jayachandran, 2019; Wang et al., 2018), Figure 2 can be reasonably explained in that when adopting a fixed cut-off frequency of 0.1 Hz, the faster velocity inevitably includes greater refractive variations into phase scintillation index during calculation. Theoretically, this unique phenomenon of "Phase without Amplitude" stems from the "Fresnel filter effect" due to different structures of the phase/amplitude power spectral densities within the lower frequency region (<the Fresnel frequency) (e.g., Rino, 1979; Strangeways et al., 2011; Wang et al., 2018).

We have tested a number of combinations of the velocity bins and corresponding number thresholds (such as 1 m/s and threshold 1, 2 m/s and threshold 2, 5 m/s and threshold 10, and 5 m/s and threshold 30), fundamentally exhibiting a similar dependence of phase scintillation index on the plasma drift with a linear slope slightly lower than 0.1 from the best fit rather than the amplitude scintillation index.

### 3.2. The Dependence of Phase Scintillation Index on the Rate of Change of TEC

Recently, several researchers have been using proxy scintillation indices developed from the estimated TEC of GNSS observables, the primary one being the rate of TEC (ROT) and rate of TEC index (ROTI) (e.g., Cherniak et al., 2022; Nie et al., 2022; Pi et al., 1997; Zhao et al., 2021). The main reason for deriving these indices is due to unavailability of high cadence data. The hypothesis for making these indices is that they are proxies for scintillation indices. If it is true, both phase and amplitude indices should depend on the proxies originated from TEC of GNSS observables. We study the possible dependencies of phase/amplitude scintillation indices on the TEC-derived parameter to test the hypothesis. In theory, the phase TEC can be precisely obtained from the carrier phase of a recorded signal wave, which is received and then processed for TEC. Hence, it is reasonable to infer that the phase variation would like to modulate the TEC change (e.g., Carrano et al., 2019). Consequently, this connection likely directs a new way to further identify the addressed presumption that the phase scintillation index ($\sigma_\varphi$) unconsciously contains the phase refractive variations, not just the diffractive variations. Below, the

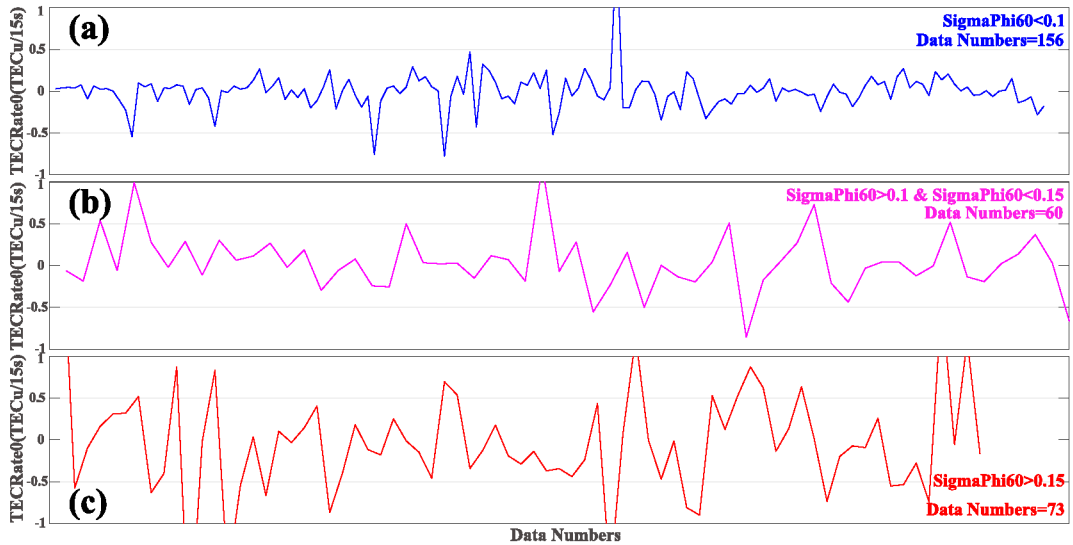


**Figure 3.** The series of rate of change of TEC (TECRate0) under three different levels of phase scintillation indices ($\sigma_\varphi$) when the plasma velocity is greater than 0.7 km/s: (a) $\sigma_\varphi < 0.1$ rad (blue line), (b) $0.1 \leq \sigma_\varphi < 0.15$ rad (magenta line), and (c) $\sigma_\varphi \geq 0.15$ rad (red line). The number of involved data triads is suggested at the right corner of each panel.

study of dependencies of phase/amplitude scintillation indices on the corresponding rate of change of TEC is first performed.

In this experiment, the already established datasets are implemented again. The rate of change of TEC is represented by TECRate0, the change of slant phase TEC in a period of 15 s, which is defined as the TEC at a given epoch minus TEC in 15 s before (such as: $TEC_0 - TEC_{-15}$, $TEC_{15} - TEC_0$, $TEC_{30} - TEC_{15}$, $TEC_{45} - TEC_{30}$ in each 1 min interval). Figure 3 shows the initial comparisons of the TECRate0 when $\sigma_\varphi$ at three different levels, in which the velocity speeds of selected data triads are fully greater than 0.7 km/s. Figure 3a represents the series of TECRate0 with $\sigma_\varphi < 0.1$ rad, Figure 3b shows the series of TECRate0 when $0.1 \leq \sigma_\varphi < 0.15$ rad, and Figure 3c exhibits the series of TECRate0 along $\sigma_\varphi \geq 0.15$ rad. The numbers at the right corner of each panel show the number of data triads. Figures 3a–3c show that the magnitude of TECRate0 increases as the $\sigma_\varphi$ becomes stronger, sketchily evidencing the dependence of the phase scintillation index on the rate of change of TEC as expected.

A statistical study is performed on the possible relationship between the scintillation indices and the rate of change of TEC. For this purpose, the data triads are completely applied to release the limitation of velocity speed, as shown in Figure 3. Referring to Figure 2, two datasets were also binned into TECRate0 by 0.008 TECu/15 s (1 TECu = $10^{16}$ electron/m$^2$) and then averaged scintillation indices ($\sigma_\varphi$ and $S_4$, respectively) when confronting a heavy amount of corresponding data triads in the datasets. To filter the singular point, the number threshold of data triads in each TECRate0 container is arbitrarily set at 5. Figure 4 exhibits the dependencies of $\sigma_\varphi$ and $S_4$ ($y$-axis) on TECRate0 ($x$-axis), upper panel for $\sigma_\varphi$, and bottom panel for $S_4$. The red squares represent the averaged scintillation indices in the corresponding TECRate0 bins. Blue vertical lines indicate the standard errors in each bin. In Figures 4a and 4b, the solid black lines show the fitting lines of quadratic polynomial and the linear least-square, respectively, based on each bin's average values, with the corresponding functional equations. From Figure 4, it is clear that phase scintillation index dependence on TECRate0 is much greater than the amplitude scintillation index. Meanwhile, regarding the absolute values of TECRate0 from Figure 4a, the positive dependence of phase scintillations index on the TECRate0 (the slope of the linear fit is around 0.2, not shown here) is nearly identical to the result from Figure 2a (with a slope of 0.11). Once again, the amplitude scintillation index is not dependent on TECRate0. The lack of dependence of $S_4$ on the rate of change of TEC reveals that the proxy indices such as the ROT/ROTI are dominated by refractive variations and, therefore, do not represent the presence of amplitude scintillation. Furthermore, the threshold, which was arbitrarily set, has been checked carefully (e.g., 0.008 TECu/15 s with threshold 0, and 0.008 TECu/15 s with threshold 2), showing almost the same results.

As a consequence, this expectancy clearly certifies the statistically positive dependence of only phase scintillation variations on the rate of change of TEC. Note that the time period of TECRate0 is 15 s, manifesting the

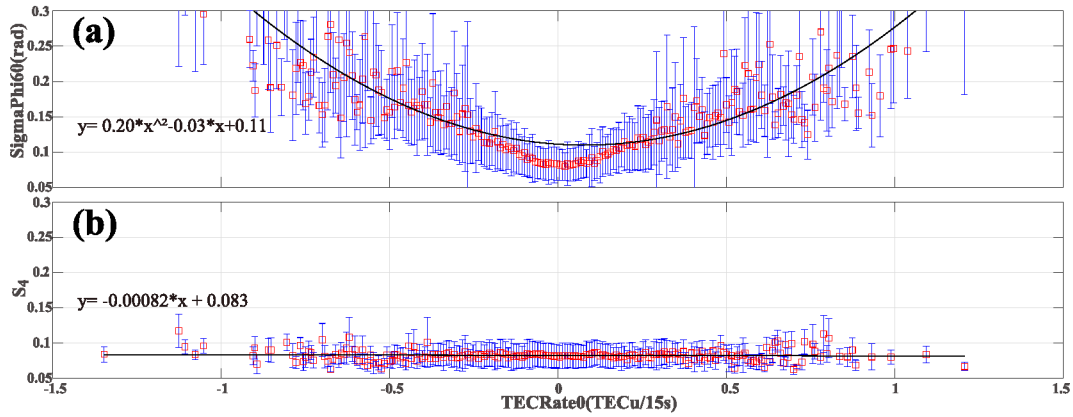


**Figure 4.** Similar as Figure 2 but on the rate of change of TEC (TECRate0). The TECRate0 is binned into the TEC bin of 0.008 TECu/15 s with a number threshold of 5. Box symbols are averaged scintillation indices in each bin and error bars are their standard deviations. The lines of best fit to the averages are presented in each panel, as well as their equations. Note that the TECRate0 is defined as the slant phase TEC at a specific time minus the corresponding TEC at the time of 15 s before (TECRate0 = $TEC_0 - TEC_{-15}$, $TEC_{15} - TEC_0$, $TEC_{30} - TEC_{15}$, and $TEC_{45} - TEC_{30}$ in each 1 min interval).

frequency of rate of change of TEC is approximately 0.067 Hz (1/15 Hz). Practically, the TEC variations with a more extended period [e.g., TECRate in 30 s (~0.03 Hz), TECRate in 1 min (~0.016 Hz)] have already been attempted to examine the dependencies of phase scintillation variations on these TECRates. The results reveal that with a longer period of the rate of change of TEC (with lower frequency), the dependence is weaker, fundamentally demonstrating that when the rate of change of TEC in a more suitable frequency, a stronger dependence of phase variation on the rate of change of TEC appears. Following this trend, we can reasonably speculate that the rate of change of TEC in a time period of 10 s (~0.1 Hz) or a slightly shorter (a higher frequency) would like to draw a closer relation to the phase scintillation variation. Because the standard scintillation indices have been processed with a fixed cut-off frequency of 0.1 Hz. Note that, in this study, the shortest time period of TEC rates we obtained is 15 s (~0.067 Hz). In the near future, it is worth to adapting the TEC perturbations with higher frequency.

## 4. Discussion

As reported by previous studies (e.g., Materassi & Mitchell, 2007; McCaffrey & Jayachandran, 2019; Oksavik et al., 2015; van der Meeren et al., 2014, 2015; Wang et al., 2018), when the radio signal passes through the ionosphere, the diffractive effect is often produced by the plasma irregularities within scale sizes from tens of meters to hundreds of meters, which are usually smaller than the Fresnel scale (e.g., Kintner et al., 2007). Meanwhile, it was well established that the refractive effect on the carrier phase of the signal wave is produced by electron densities with larger scales (smaller frequency) in the ionosphere. Typically, for GPS L-band signal at an assumed height of 350 km, the Fresnel scale is approximately 360 m both for amplitude and phase (Forte & Radicella, 2002). As we know, the Fresnel scale is a critical parameter when dealing with the scintillations from GNSS data, which is sensitive to the relative drift velocity (e.g., Forte & Radicella, 2002; Pi et al., 1997; Strangeways et al., 2011). Note that the relative drift velocity is a composed vector from the ionospheric plasma flow to the movement of the ray path of the satellite at the ionosphere, which is dominantly controlled by the high-speed plasma flow in particular at high latitudes.

As addressed, the refractive variations are produced mainly by the larger-scale structures with a relatively lower frequency. Nevertheless, when the relative drift velocity is going higher in particular over the polar region, the frequency of refractive variations can certainly exceed 0.1 Hz (often defined as the cut-off frequency for automatically detrending), which will be mistakenly considered as the diffraction scintillation and then are logically represented by the scintillation indices.

As a consequence, the Fresnel frequency should be properly determined in order to remove refractive fluctuations from the truth scintillation accurately. Otherwise, the phase refractive variations will be inevitably included in the scintillation analysis much more than the amplitude variations due to their differentiated distributions of power

spectral density below the Fresnel frequency, very probably making the famous "Phase without Amplitude" scintillations. In contrast, if the signal is appropriately processed together with an adequate frequency or when the 0.1 Hz is valid, the scintillations of phase and amplitude will come out together, fundamentally originating from the diffraction pattern induced by the ionospheric plasma irregularities (Jayachandran et al., 2017).

In literature, Wang et al. (2018) presented the first-ever experimental evidence to clearly demonstrate a strong dependence of $\sigma_\varphi$ on the increased plasma drift speed at the noon sector. In this study, we provide more evidence at the dawn sector to further prove the stated dependence (Figure 2). In comparison with these two experiments, the linear dependence (the slope in best fit) at the noon sector is slightly greater than that on the dawn sector, which can be properly explained by the general recognition that the occurrence of high-speed velocity is statistically greater than that at the dawn sector. Hence, it provides one more positive evidence to support the dependence, reminding us to carefully treat the phase scintillation index in particular when encountering the high plasma flow.

Actually, other than the plasma velocity, one more parameter has been comprehensively employed to check the possible relations of phase variations on them. Hereby, Figure 3 qualifies that the rate of change of TECs are intuitively growing along with the increasing phase scintillation indices. Figure 4 shows a clear statistical positive correlation of phase fluctuations on TECRate0 (the rate of change of TEC in an interval of 15 s). Generally speaking, with the increasing TECRate0 (absolute values), the phase scintillation indices are linearly growing with a slope of best fit around 0.2. It can be simply explained by that more power, carried by the greater TECRate0-related irregularities (at lower frequency), definitely produce stronger intensities of phase refractive variations, which is naturally thought as the phase scintillation and then represented by the standard phase scintillation index. However, the amplitude scintillation index does not depend on the TECRate0. As mentioned above, the frequency of involved TECRate0 is just around 0.067 Hz, which is lightly lower than the fixed cut-off frequency (0.1 Hz). The results presented here implies that the proxy scintillation indices such as ROT/ROTI (e.g., Carrano et al., 2019) are dominated by the refractive contributions and therefore cannot be used to represent amplitude scintillation.

These dependencies of standard phase scintillation indices on the parameters of velocity speed and rate of change of TEC can be used to construct a quickly empirical predication model. When we just obtain one parameter among them, the anticipations of the other two parameters can be roughly given (e.g., Carrano et al., 2016).

## 5. Conclusion

In this study, we present further proof to confirm the linear dependencies of the standard phase scintillation index ($\sigma_\varphi$) on the parameters of flow drift speed and rate of change of TEC around the dawn sector of the polar region. The identified dependencies could be fundamentally explained by that the phase refractive variations led to the standard phase scintillation index when detrending the GNSS data automatically with a fixed cut-off frequency (0.1 Hz). As a consequence, our results not only emphasize the importance of paying extreme attention to using the phase scintillation index at the high latitudes, but also remind us to carefully choose the crucial cut-off frequency (considered as the Fresnel frequency) in detrending the GNSS data. In addition, it provides a good opportunity to quickly establish an empirical model to forecast the corresponding parameters in anticipation over the polar region. The study also shows that proxy scintillation indices such as ROT/ROTI are dominated by refractive effects and therefore do not adequately account for the presence of amplitude scintillation.

## Data Availability Statement

The data of GPS receiver is provided by the CHAIN from the database (http://chain.physics.unb.ca/chain/). The SuperDARN radar data are provided by Virginia Tech. through the website (http://vt.superdarn.org/tiki-index.php).

**Acknowledgments**
This work in China is supported by National Natural Science Foundation (Grant 41574138, 41274149, 41604139), China Postdoctoral Science Foundation funded project (2020M682163), the International Partnership Program of Chinese Academy of Sciences (Grant 183311KYSB20200003), and the Chinese Meridian Project. The authors are grateful for support from the ISSI/ISSI-BJ workshop "Multi-Scale Magnetosphere-Ionosphere-Thermosphere Interaction." Infrastructure funding for CHAIN was provided by the Canadian Foundation for Innovation and the New Brunswick Innovation Foundation. CHAIN operations are conducted in collaboration with the Canadian Space Agency. This research was undertaken with the financial support of the Canadian Space Agency FAST program and the Natural Sciences and Engineering Research Council of Canada. The SuperDARN is a collection of radars funded by national scientific funding agencies of Australia, Canada, China, France, Japan, South Africa, the United Kingdom, and the United States of America. The HF radars of Blackstone and Fort Hays West are operated by Virginia Tech. The Christmas Valley East HF radar is maintained by Dartmouth College.

## References

Beach, L. T. (2006). Perils of the GPS phase scintillation index ($\sigma_\varphi$). *Radio Science*, *41*, RS5S31. https://doi.org/10.1029/2005RS003356

Carrano, C. S., Groves, K. M., & Rino, C. L. (2019). On the relationship between the rate of change of total electron content index (ROTI), irregularity strength ($C_k$L), and the scintillation index ($S_4$). *Journal of Geophysical Research: Space Physics*, *124*, 2099–2112. https://doi.org/10.1029/2018JA026353

Carrano, C. S., Groves, K. M., Rino, C. L., & Doherty, P. H. (2016). A technique for inferring zonal irregularity drift from single-station GNSS measurements of intensity ($S_4$) and phase ($\sigma_\phi$) scintillations. *Radio Science*, *51*, 1263–1277. https://doi.org/10.1002/2015RS005864

Cherniak, I., Zakharenkova, I., & Krankowski, A. (2022). IGS ROTI maps: Current status and its extension towards equatorial region and southern hemisphere. *Sensors*, *22*(3748), 1–17. https://doi.org/10.3390/s22103748

Chisham, G., Lester, M., Milan, S. E., Freeman, M. P., Bristow, W. A., Grocott, A., et al. (2007). A decade of the Super Dual Auroral Radar Network (SuperDARN): Scientific achievements, new techniques and future directions. *Surveys in Geophysics*, *28*, 33–109. https://doi.org/10.1007/s10712-007-9017-8

Doherty, P. H., Delay, S. H., Valladares, C. E., & Klobuchar, J. A. (2003). Ionospheric scintillation effects in the equatorial and auroral regions. *Journal of the Institute of Navigation*, *50*(4), 2003–2004. https://doi.org/10.1002/j.2161-4296.2003.tb00332.x

Forte, B. (2005). Optimum detrending of raw GPS data for scintillation measurements at auroral latitudes. *Journal of Atmospheric and Terrestrial Physics*, *67*, 1100–1109. https://doi.org/10.1016/j.jastp.2005.01.011

Forte, B., & Radicella, S. M. (2002). Problems in data treatment for ionospheric scintillation measurements. *Radio Science*, *37*(6), 1096. https://doi.org/10.1029/2001RS002508

Fremouw, E. J., Leadabrand, R. L., Livingston, R. C., Cousins, M. D., Rino, C. L., Fair, B. C., & Long, R. A. (1978). Early results from the DNA Wideband satellite experiment: Complex signal scintillation. *Radio Science*, *13*(1), 167–187. https://doi.org/10.1029/RS013i001p00167

Greenwald, R. A., Bristow, W. A., Sofko, G. J., Senior, C., Cerisier, J.-C., & Szabo, A. (1995). Super dual auroral radar network radar imaging of dayside high-latitude convection under northward interplanetary magnetic field: Toward resolving the distorted two-cell versus multicell controversy. *Journal of Geophysical Research*, *100*(A10), 19661–19674. https://doi.org/10.1029/95JA01215

Hey, J. S., Parsons, S. J., & Phillips, J. W. (1946). Fluctuations in cosmic radiation at radio-frequencies. *Nature*, *158*, 234. https://doi.org/10.1038/158234a0

Jayachandran, P. T., Hamza, A. M., Hosokawa, K., Mezaoui, H., & Shiokawa, K. (2017). GPS amplitude and phase scintillation associated with polar cap auroral forms. *Journal of Atmospheric and Terrestrial Physics*, *164*, 185–191. https://doi.org/10.1016/j.jastp.2017.08.030

Jayachandran, P. T., Langley, R. B., MacDougall, J. W., Mushini, S. C., Pokhotelov, D., Hamza, A. M., et al. (2009). Canadian High Arctic Ionospheric Network (CHAIN). *Radio Science*, *44*, RS0A03. https://doi.org/10.1029/2008rs004046

Kintner, P. M., Ledvina, B. M., & de Paula, E. R. (2007). GPS and ionospheric scintillations. *Space Weather*, *5*, S09003. https://doi.org/10.1029/2006SW000260

Li, G., Ning, B., Hu, L., Liu, L., Yue, X., Wan, W., et al. (2010). Longitudinal development of low-latitude ionospheric irregularities during the geomagnetic storms of July 2004. *Journal of Geophysical Research*, *115*, A04304. https://doi.org/10.1029/2009JA014830

Liu, J., Lyons, L. R., Wang, C. P., Hairston, M. R., Zhang, Y., & Zou, Y. (2020). Dawnside auroral polarization streams. *Journal of Geophysical Research: Space Physics*, *125*, e2019JA027742. https://doi.org/10.1029/2019JA027742

Materassi, M., Alfonsi, L., De Franceschi, G., Romano, V., Mitchell, C., & Spalla, P. (2009). Detrend effect on the scalograms of GPS power scintillation. *Advances in Space Research*, *43*(11), 1740–1748. https://doi.org/10.1016/j.asr.2008.01.023

Materassi, M., & Mitchell, C. N. (2007). Wavelet analysis of GPS amplitude scintillation: A case study. *Radio Science*, *42*, RS1004. https://doi.org/10.1029/2005RS003415

McCaffrey, A. M., & Jayachandran, P. T. (2019). Determination of the refractive contribution to GPS phase "scintillation". *Journal of Geophysical Research: Space Physics*, *124*, 1454–1469. https://doi.org/10.1029/2018JA025759

Mitchell, C. N., Alfonsi, L., De Franceschi, G., Lester, M., Romano, V., & Wernik, A. W. (2005). GPS TEC and scintillation measurements from the polar ionosphere during the October 2003 storm. *Geophysical Research Letters*, *32*, L12S03. https://doi.org/10.1029/2004GL021644

Moen, J., Oksavik, K., Alfonsi, L., Daabakk, Y., Romano, V., & Spogli, L. (2013). Space weather challenges of the polar cap ionosphere. *Journal of Space Weather and Space Climate*, *3*, A02. https://doi.org/10.1051/SWSC/2013025

Mushini, S. C., Jayachandran, P. T., Langley, R. B., MacDougall, J. W., & Pokhotelov, D. (2012). Improved amplitude- and phase-scintillation indices derived from wavelet detrended high-latitude GPS data. *GPS Solutions*, *16*(3), 363–373. https://doi.org/10.1007/s10291-011-0238-4

Nie, W. F., Rovira-Garcia, A., Li, M., Fang, Z., Wang, Y., Zheng, D., & Xu, T. (2022). The mechanism for GNSS-based kinematic positioning degradation at high-latitudes under the March 2015 great storm. *Space Weather*, *20*(6), e2022SW003132. https://doi.org/10.1029/2022SW003132

Oksavik, K., vander Meeren, C., Lorentzen, D. A., Baddeley, L. J., & Moen, J. (2015). Scintillation and loss of signal lock from poleward moving auroral forms in the cusp ionosphere. *Journal of Geophysical Research: Space Physics*, *120*, 9161–9175. https://doi.org/10.1002/2015JA021528

Pi, X., Boulat, B., Mannucci, A. J., Reyes, M., & Stowers, D. (2001). *Ionospheric scintillations measured using GPS receivers during the current solar maximum*. International Beacon Satellite Symposium, Boston.

Pi, X., Mannucci, A. J., Lindqwister, U. J., & Ho, C. M. (1997). Monitoring of global ionospheric irregularities using the worldwide GPS network. *Geophysical Research Letters*, *24*(18), 2283–2286. https://doi.org/10.1029/97GL02273

Rino, C. L. (1979). A power law phase screen model for ionospheric scintillation, 1. Weak scatter. *Radio Science*, *14*(6), 1135–1145. https://doi.org/10.1029/RS014i006p01135

Ruohoniemi, J. M., & Baker, K. B. (1998). Large-scale imaging of high-latitude convection with SuperDARN HF radar observations. *Journal of Geophysical Research*, *103*(A9), 20797–20811. https://doi.org/10.1029/98JA01288

Shepherd, S. G., & Ruohoniemi, J. M. (2000). Electrostatic potential patterns in the high-latitude ionosphere constrained by SuperDARN measurements. *Journal of Geophysical Research*, *105*(A10), 23005–23014. https://doi.org/10.1029/2000JA000171

Strangeways, H. J., Ho, Y.-H., Aquino, M. H. O., Elmas, Z. G., Marques, H. A., Monico, J. F. G., & Silva, H. A. (2011). On determining spectral parameters, tracking jitter, and GPS positioning improvement by scintillation mitigation. *Radio Science*, *46*, RS0D15. https://doi.org/10.1029/2010RS004575

van der Meeren, C., Oksavik, K., Lorentzen, D., Moen, J. I., & Romano, V. (2014). GPS scintillation and irregularities at the front of an ionization tongue in the nightside polar ionosphere. *Journal of Geophysical Research: Space Physics*, *119*, 8624–8636. https://doi.org/10.1002/2014JA020114

van der Meeren, C., Oksavik, K., Lorentzen, D. A., Rietveld, M. T., & Clausen, L. B. N. (2015). Severe and localized GNSS scintillation at the poleward edge of the nightside auroral oval during intense substorm aurora. *Journal of Geophysical Research: Space Physics*, *120*, 10607–10621. https://doi.org/10.1002/2015JA021819

Van Dierendonck, A. J., Klobuchar, J. A., & Hua, Q. (1993). *Ionospheric scintillation monitoring using commercial single frequency C/A code receivers*. Paper presented at ION GPS- 93. Inst. of Navigat.

Wang, Y., Cao, Z., Xing, Z.-Y., Zhang, Q.-H., Jayachandran, P. T., Oksavik, K., et al. (2021). GPS scintillations and TEC variations in association with a polar cap arc. *Journal of Geophysical Research: Space Physics*, *126*, e2020JA028968. https://doi.org/10.1029/2020JA028968

Wang, Y., Zhang, Q.-H., Jayachandran, P. T., Lockwood, M., Zhang, S.-R., Moen, J., et al. (2016). A comparison between large-scale irregularities and scintillations in the polar ionosphere. *Geophysical Research Letters*, *43*, 4790–4798. https://doi.org/10.1002/2016GL069230

Wang, Y., Zhang, Q.-H., Jayachandran, P. T., Moen, J., Xing, Z.-Y., Chadwick, R., et al. (2018). Experimental evidence on the dependence of the standard GPS phase scintillation index on the ionospheric plasma drift around noon sector of the polar ionosphere. *Journal of Geophysical Research: Space Physics*, *123*, 2370–2378. https://doi.org/10.1002/2017JA024805

Wang, Y., Zhang, Q.-H., Ma, Y.-Z., Jayachandran, P. T., Xing, Z.-Y., Balan, N., & Zhang, S.-R. (2020). Polar ionospheric large-scale structures and dynamics revealed by TEC keogram extracted from TEC maps. *Journal of Geophysical Research: Space Physics*, *125*, e2019JA027020. https://doi.org/10.1029/2019JA027020

Weber, E. J., Klobuchar, J. A., Buchau, J., Carlson, H. C. Jr., Livingston, R. C., de la Beaujardiere, O., et al. (1986). Polar cap F layer patches: Structure and dynamics. *Journal of Geophysical Research*, *91*(A11), 12121–12129. https://doi.org/10.1029/JA091iA11p12121

Zhang, Q.-H., Zhang, B.-C., Lockwood, M., Hu, H.-Q., Moen, J., Michael Ruohoniemi, J., et al. (2013). Direct observations of the evolution of polar cap ionization patches. *Science*, *339*, 1597–1600. https://doi.org/10.1126/science.1231487

Zhao, D. S., Li, W., Li, C., Tang, X., Wang, Q., Hancock, C. M., et al. (2021). Ionospheric phase scintillation index estimation based on 1 Hz geodetic GNSS receiver measurements by using continuous wavelet transform. *Space Weather*, *20*, e2021SW003015. https://doi.org/10.1029/2021SW003015